these worms express readily detectable reporter products, whereas controls show minimal expression[4].

Worms were exposed overnight to continuous-wave microwave radiation at 750 MHz and 0.5 W in the transverse electromagnetic (TEM) cell described previously[5]. Figure 1 shows temperature profiles for reporter expression in both irradiated and control (foil-shielded) worm cultures. In microwave-exposed cultures, expression is comparable to that of controls at 24.0 °C ($P > 0.05$), but then rises steeply through 24.5 and 25.0 to 25.5 °C ($P < 0.001$). In non-exposed controls, heat-induced reporter expression follows the pattern for HSP16 (ref. 6), increasing sharply only above 27 °C (to a maximum at 30 °C). There is thus a disparity of 3 °C between exposed and control induction profiles.

A thermal explanation for this disparity would require that the exposed worms become 3 °C warmer than controls — or more if only a minority of worms/tissues is affected. We reject this thermal explanation on several grounds, not least the diffusion of heat over 18 hours.

First, no temperature difference is detectable between control and exposed cultures after irradiation[5]. This is also true for concentrated (50% w/v) worm suspensions incubated for 18 h at 25 °C alongside a saline solution alone, under exposed versus control conditions (24.68 ± 0.116 °C s.d., $P = 0.28$, for all 16 measurements under four conditions using a sensitive copper–constantan microthermocouple). Temperature differences of 0.5 °C (that is, worms 1 °C warmer than the saline) would have been easily detectable in this experiment.

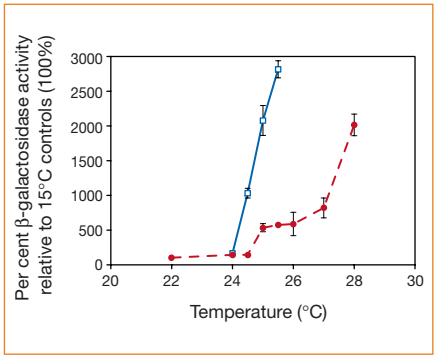

Figure 1 Saline[9] suspensions of young adult PC72 worms grown synchronously at 15 °C (ref. 10) were split between three conditions for a total of 18 h: (1) exposed to microwaves (in TEM cell at 750 MHz and 0.5 W; ref. 5) within a Leec LT3 incubator; (2) temperature controls shielded with aluminium foil in the same incubator; (3) baseline controls at 15 °C. Incubator temperatures of 24.0, 24.5, 25.0 and 25.5 °C were tested using 12 replicates for each condition; controls only (6 replicates of condition 2) were also run at 22, 26, 27 and 28 °C. All worm samples were assayed fluorometrically[4,5] for β-galactosidase activity. Enzyme activities were normalized against 15 °C baseline controls (100%) within each batch to allow comparison of reporter induction at different temperatures. Squares, blue solid line; reporter activities (± s.e.m.) in microwave-exposed cultures. Circles, red dashed line; control reporter activities (± s.e.m.) at each temperature.

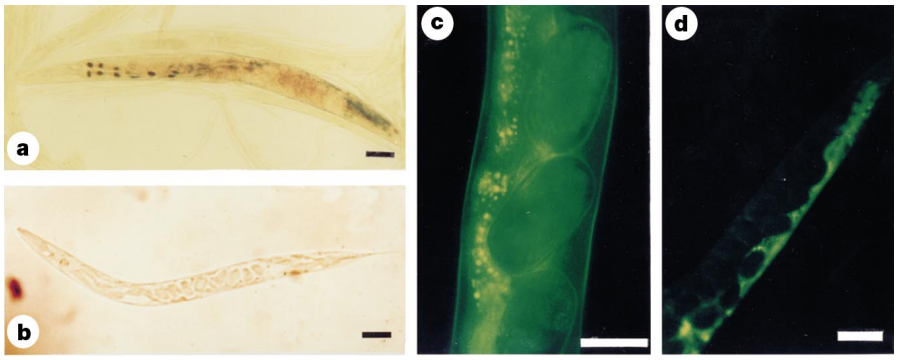

Figure 2 PC72 and PC161 (similar to PC72, but carrying an additional GFP reporter under *hsp16* control) worms were either exposed for 18 h at 25 °C to microwaves (750 MHz, 0.5 W) or kept as 25 °C controls, then reporter expression was localized *in situ* by staining with X-gal (PC72) or viewing under ultraviolet light on a fluorescence microscope (PC161). **a,** Exposed PC72 worm, showing nuclear staining for β-galactosidase throughout the gut; **b,** typical PC72 worm under control conditions: no observable staining; **c,** exposed PC161 worm, showing GFP fluorescence throughout ovoid embryos; **d,** typical control PC161 worm, showing yellowish gut autofluorescence (also in **c**) but no GFP fluorescence in embryos. Note that many worms in **a** and **c** show little reporter expression. Scale bars, 50 μm.

Second, *in situ* detection of reporter products shows that *lacZ* is expressed throughout the gut in PC72 worms (Fig. 2a,b), and also that GFP is expressed in many embryos within adult PC161 worms (Fig. 2c,d). These expression sites together constitute about half of worm tissues.

Third, the field at the centre of our TEM cell is 45 V m^{-1}, and the measured permittivity of concentrated worm suspensions (at 615 MHz) gives a conductivity of about 0.48 Ω^{-1} m^{-1}. The calculated specific absorption rate (SAR) is only 0.001 W kg^{-1}, which is much less than published values[7] for mobile phones (0.02–1.0 W kg^{-1}). Mobile-phone manufacturers claim that SARs in this range are insufficient to cause measurable tissue heating within the human head, and we are not disputing this.

We suggest instead that the induction of heat-shock proteins described here could involve non-thermal mechanisms. These could include microwave disruption of the weak bonds that maintain the active folded forms of proteins; enhanced production of reactive oxygen species (known to be inducers of HSPs[8]); or interference with cell-signalling pathways that affect HSP induction (by heat-shock-factor activation). All these mechanisms are testable using the functional genomic tools that are available in *C. elegans*. Because of the universality of the heat-shock response[2], a similar non-thermal induction might also occur in human tissues exposed to microwaves, a possibility that needs investigation.

David de Pomerai*, Clare Daniells*, Helen David*, Joanna Allan*, Ian Duce*, Mohammed Mutwakil*, David Thomas†, Phillip Sewell†, John Tattersall‡, Don Jones§, Peter Candido§

**Molecular Toxicology Division, School of Biological Sciences and* †*School of Electrical and Electronic Engineering, University of Nottingham, Nottingham NG7 2RD, UK*

‡*Medical Countermeasures, CBD Porton Down, Salisbury, Wiltshire SP4 0JQ, UK*

§*Department of Biochemistry and Molecular Biology, University of British Columbia, 2146 Health Sciences Mall, Vancouver V6T 1Z3, Canada*

1. ANSI/IEEE C95.1-1992 *American National Standard-Safety Levels with Respect to Exposure to Radio Frequency Electromagnetic Fields, 3 kHz to 300 GHz* (IEEE, New York, 1992).
2. Parsell, D. & Lindquist, S. *Annu. Rev. Genet.* **27,** 437–496 (1993).
3. Dennis, J., Mutawakil, M., Lowe, K. & de Pomerai, D. *Aquatic Toxicol.* **40,** 37–50 (1997).
4. Candido, E. & Jones, D. *Trends Biotechnol.* **40,** 125–129 (1996).
5. Daniells, C. *et al. Mutat. Res.* **399,** 55–64 (1998).
6. Snutch, T. & Baillie, D. *Can. J. Biochem. Cell Biol.* **61,** 480–487 (1983).
7. Gandhi, O., Lazzi, G. & Furse, C. *IEEE Trans. Microwave Theor. Tech.* **44,** 1884–1897 (1996).
8. Nishizawa, J. *et al. Circulation* **99,** 934–941 (1999).
9. Williams, P. & Dusenbery, D. *Environ. Toxicol. Chem.* **9,** 1285–1290 (1990).
10. Jewitt, N., Anthony, P., Lowe, K. & de Pomerai, D. *Enzyme Microb. Technol.* **25,** 349–356 (1999).

Structural biology

Proton-powered turbine of a plant motor

ATP synthases are enzymes that can work in two directions to catalyse either the synthesis or breakdown of ATP, and they constitute the smallest rotary motors in biology. The flow of protons propels the rotation[1] of a membrane-spanning complex of identical protein subunits, the number of which determines the efficiency of energy conversion. This proton-powered turbine is predicted to consist of 12 subunits[2–4], based on data for *Escherichia coli*[5]. The yeast mitochondrial enzyme, however, has only 10 subunits[6]. We have imaged the ATP synthase from leaf chloroplasts by using atomic force microscopy and, surprisingly, find that its turbine has 14 subunits, arranged in a cylindrical ring.

We isolated the rotating oligomer from spinach-chloroplast ATP synthase enzyme preparations and reconstituted it at a high protein-to-lipid ratio in two-dimensional arrays. During the detergent-mediated procedure, the membrane-embedded oligomer remains intact (relative molecular mass 100K; individual subunits, known as subunits III, are 8.0K, and are equivalent to subunit-*c* in mitochondria and bacteria). The flanking stator proteins I, II and IV of this turbine, as well as all subunits ($\alpha_3\beta_3\gamma\delta\epsilon$) of the ATP-generating hydrophilic portion of the enzyme (known as F_1), are absent (Fig. 1a).

Imaging the topography of the densely packed subunit-III$_x$ oligomers by contact-mode atomic force microscopy reveals alternating ring-like structures of two different diameters (Fig. 2). The narrow and the wider rings of the subunit-III oligomers have outer diameters of 5.9 ± 0.3 nm and 7.4 ± 0.3 nm, respectively. Both orifices have inner diameters of 3.5 ± 0.3 nm. Only a single, sharp band, corresponding to a relative molecular mass of 100K, is resolved on SDS–polyacrylamide gels of the protein arrays, which is the size expected for the subunit-III$_x$ oligomer of the native ATP synthase from chloroplasts (Fig. 1a), indicating that most of the oligomers must have the same stoichiometry.

We conclude that the adjacent wide and narrow rings represent the two channel entrances of III$_x$ oligomers, with opposite orientations perpendicular to the membrane surface (Fig. 2). The individual subunits of the 7.4-nm-diameter orifice protrude by 1.7 ± 0.3 nm from the bilayer surface, whereas those of the 5.9-nm-diameter orifice protrude by 1.5 ± 0.3 nm; the oligomer, which is 7.3 ± 0.3 nm long, traverses the lipid bilayer (thickness, 4.1 ± 0.2 nm). Two III$_x$ oligomers with wide orifices and two with narrow orifices are enlarged to display their substructure in more detail (Fig. 2). In most cases, 14 subunits per oligomer can be counted from the recorded images.

To determine the precise number of subunits in the circular III$_x$ complex, we calculated angular power spectra from 320 individual images of well-preserved particles, which yielded a distinct single peak at 14-fold symmetry (Fig. 1c; filled circles). We then averaged data from the wide rings and the narrow rings (Fig. 1b) and their respective angular power spectra revealed the 14-fold symmetry. There was a weaker 12-fold signal (22% of the 14-fold power) still present, but no significant 7-fold to 13-fold symmetric contribution (Fig. 1c). This 14-fold symmetry and the same subunit-III oligomer dimensions were also evident in samples prepared by a different method (from Coomassie-blue non-denaturing gels without SDS), in which the stator protein IV was retained (data not shown).

We conclude that the proton turbine in the F_o stem of chloroplast ATP synthase is an asymmetric cylindrical structure with 14 symmetrically distributed subunits that protrude from both membrane surfaces (Fig. 2).

So far the number of subunits, and therefore the diameter of the proton turbine, seems to be species-dependent[5,6]. Subunit stoichiometry might even vary with metabolic state within the same organism, as indicated by biochemical studies on *E. coli*[7]. The proposed elasticity of the transmission between F_o and F_1 could accommodate such a variable stoichiometry[8], as well as a non-integral H^+/ATP ratio caused by symmetry mismatch between the three-fold symmetry of catalytic sites in F_1 and the 14-fold (10-fold[6]) symmetry of the F_o oligomer.

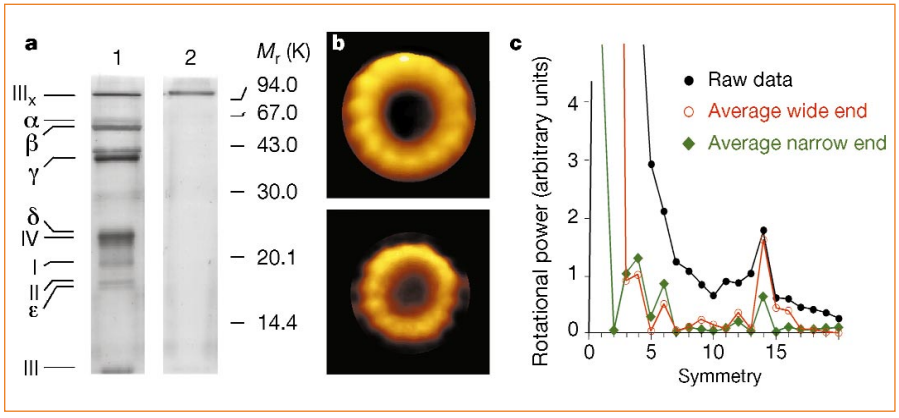

Figure 1 Characterization of subunit-III oligomers. **a,** SDS–PAGE and silver staining of chloroplast ATP synthase samples before and after reconstitution. Lane 1, the ATP synthase: proteins of the F_1 complex are designated by Greek letters, those of the F_o complex by roman numerals. The sample was incubated in SDS buffer at 50 °C for 10 min to dissociate part of the III$_x$ oligomer into its 8K monomers for reference. Lane 2, in reconstituted protein arrays, as used for atomic force microscopy, only the 100K III$_x$ oligomer is present. To isolate intact subunit-III oligomers, SDS detergent[9] was added to the CF_oF_1 complex obtained from rate-zonal centrifugation[10] and then replaced with dodecyl maltoside detergent. The III$_x$ oligomer was reconstituted into lipid bilayers (phosphatidylcholine and phosphatidic acid from egg yolk) by removing detergent with BioBeads SM2 (Bio-Rad, Hercules, California). **b,** Averaged topographs of the wide (top; $n = 220$) and narrow (bottom; $n = 220$) oligomer ends, generated by reference-free translational and rotational alignment of the individual particles. **c,** Rotational power spectra calculated from 320 topographs of individual oligomers (filled circles) and of averaged wide (circles) and narrow (diamonds) rings. The four-fold contribution of the spectra is due to the four neighbouring complexes in the crystal.

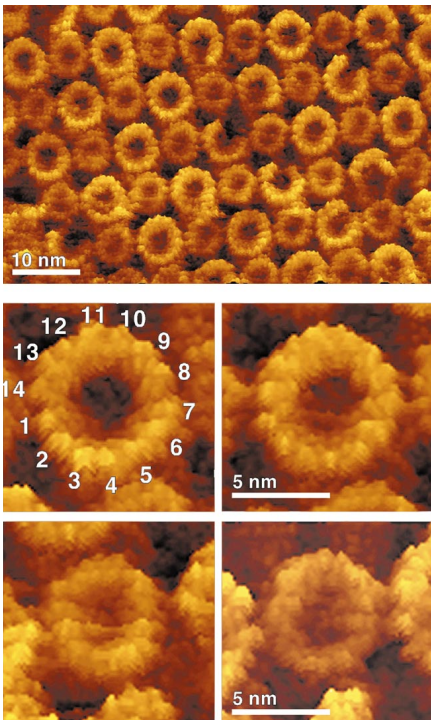

Figure 2 Subunit-III oligomers of chloroplast ATP synthase visualized in 25 mM $MgCl_2$, 10 mM Tris–HCl, pH 7.8, at room temperature using atomic force microscopy (Nanoscope III, Digital Instruments)[11]. Top, the distinct wide and narrow rings represent the two surfaces of the subunit-III$_x$ oligomer; middle, wide oligomer ends, showing 14 subunits-III; bottom, narrow oligomer ends. The full grey-level range of these topographs was 2 nm.

Holger Seelert*, Ansgar Poetsch*, Norbert A. Dencher*, Andreas Engel†, Henning Stahlberg†, Daniel J. Müller†‡

**Physical Biochemistry, Department of Chemistry, Darmstadt University of Technology, D-64287 Darmstadt, Germany*
e-mail: dencher@pop.tu-darmstadt.de
†M. E. Müller-Institute for Structural Biology, Biozentrum, University of Basel, CH-4056 Basel, Switzerland
‡Max-Planck-Institute of Molecular Cell Biology and Genetics, D-01307 Dresden, Germany

1. Sambongi, Y. *et al. Science* **286,** 1722–1724 (1999).
2. Junge, W. *Proc. Natl Acad. Sci. USA* **96,** 4735–4737 (1999).
3. Dimroth, P., Wang, H., Grabe, M. & Oster, G. *Proc. Natl Acad. Sci. USA* **96,** 4924–4929 (1999).
4. Rastogi, V. K. & Girvin, M. E. *Nature* **402,** 263–268 (1999).
5. Jones, P. C. & Fillingame, R. H. *J. Biol. Chem.* **273,** 29701–29705 (1998).
6. Stock, D., Leslie, A. G. W. & Walker, J. W. *Science* **286,** 1700–1705 (1999).
7. Schemidt, R. A., Qu, J., Williams, J. R. & Brusilow, W. S. A. *J. Bacteriol.* **180,** 3205–3208 (1998).
8. Cherepanov, D. A., Mulkidjanian, A. Y. & Junge, W. *FEBS Lett.* **449,** 1–6 (1999).
9. Fromme, P., Boekema, E. J. & Gräber, P. *Z. Naturforsch.* **42C,** 1239–1245 (1987).
10. Neff, D. *et al. J. Struct. Biol.* **119,** 139–148 (1997).
11. Müller, D. J., Fotiadis, D., Scheuring, S., Müller, S. A. & Engel, A. *Biophys. J.* **76,** 1101–1111 (1999).